ELSEVIER

International Journal of Heat and Fluid Flow 21 (2000) 471–479

International Journal of HEAT AND FLUID FLOW

www.elsevier.com/locate/ijhff

Near-wall behaviour of statistical properties in turbulent flows

M. Fischer *, J. Jovanović, F. Durst

Lehrstuhl für Strömungsmechanik, University of Erlangen-Nürnberg, Cauerstr. 4, 91058 Erlangen, Germany

Abstract

Many technically relevant flows are wall-bounded flows at high Reynolds numbers. The knowledge of the near-wall behaviour of turbulence is important for the correct modelling of these flows. The influence of the Reynolds number on turbulence quantities results from the imposed boundary conditions at the edge of a boundary layer or on the axis of a channel or a pipe flow. This has often been assumed not to affect the near-wall region. However, experimental and numerical results show a Reynolds number dependence of turbulence intensity very close to the wall. In this work the low-Reynolds number effects in turbulent wall-bounded flows were investigated experimentally using the LDA measuring technique. A new method is explained how to eliminate the influence of the limited spatial resolution of the LDA measuring technique.

1. Introduction

In turbulent flows at high Reynolds numbers the influence of the viscosity on technically relevant quantities is negligible. In the immediate proximity of a wall however, there is always a region where the local Reynolds numbers are small. The mechanisms of near wall turbulence can be investigated from two complementary points of view. On the one hand one can try to understand the causes of the onset of turbulence at low Reynolds numbers or on the other hand one can ask questions which concern the fully developed state of turbulence and its interaction with walls.

Although wall-bounded flows have been investigated by many researchers in the last 60 years the overall progress achieved in the field is slow. In part this is due to the lack of appropriate data which could be used to analyse the complete dynamic equations for the turbulence correlations. With advances in computer technology, it has become feasible to study turbulent flows by applying numerical techniques. Direct numerical simulations are restricted to Reynolds numbers which are far below those of technical application. Although there is general agreement in the literature about scaling of the mean velocity distribution close to the wall, there is no physical explanation for the numerically and experimentally observed variations of the fluctuating quantities when non-dimensionalized using the wall variables. In the region very close to the wall the gradients of time-averaged quantities are very high; therefore, it is not clear whether the observed Reynolds number dependences are physically real or just artefacts related to the data accuracy and the spatial resolution in experimental and numerical investigations. The goal of this work was to investigate the influence of the Reynolds number in the near-wall region of fully developed flows. We will focus our attention primarily on the region of viscous sublayer adjacent to the wall where it is expected that inner scaling laws should hold by definition for all turbulence quantities.

The laser-Doppler (LDA) measuring technique allows accurate experimental data to be obtained deep in the viscous sublayer provided that the influence of the finite size of the LDA control volume is taken into account. By measuring with different LDA volume sizes, high reliability of the turbulence data can be achieved close to the wall even at higher Reynolds numbers.

2. Implications of boundary layer transition on near-wall turbulence

Hinze (1975) concluded, from early visualization experiments of Fage and Townend (1932), that flow in the viscous sublayer is almost two-dimensional and two-component over fairly long periods of time. He also argued that there is considerable similarity between the mechanisms leading to a transition from laminar to turbulent flow and of continuous generation of turbulence in wall-bounded flows. These inferences, deduced from the accumulated experimental data, suggest that we can apply some knowledge of the linear theory of hydromechanical stability, which describes the so-called Tollmien–Schlichting type of turbulence, to access the properties of the flow structures close to the wall. As demonstrated by flow visualization experiments of Kline et al. (1967), organized structures in the form thin streak filaments shown in Fig. 1 play a key role in the continuous generation of turbulence near the walls.

Assuming that the flow pattern within the streak filament is initially laminar, undergoing some sort of transition process (see Kim et al., 1971), we can make an attempt to deduce the

* Corresponding author. Tel.: +49-9131-8528291; fax: +49-9131-8529503.

E-mail address: mfischer@lstm.uni-erlangen.de (M. Fischer).

0142-727X/00/$ - see front matter
PII: S0142-727X(00)00034-5

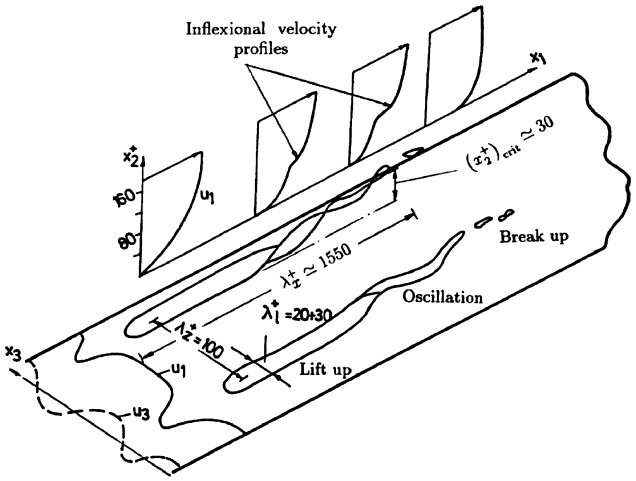

Fig. 1. The structure of turbulence close to the wall and the length scales deduced from transitional instability.

characteristic length and time scales of this structure using the critical Reynolds number (defined at the instability point) valid for laminar boundary layers (see Schlichting, 1968):

$$\left(\frac{U_\infty \delta_1}{\nu}\right)_{\text{crit}} = 520, \tag{1}$$

where δ_1 and U_∞ represent the displacement thickness and velocity at the edge of the shear layer. Using the relationships for the boundary layer thickness δ_1 and the skin friction coefficient c_f:

$$\delta_1 = 1.7208\sqrt{\frac{\nu x}{U_\infty}} \quad \text{and} \quad c_f = \frac{\tau_0}{(1/2)\rho U_\infty^2} = \frac{0.332}{\sqrt{(U_\infty x/\nu)}} \tag{2}$$

the following estimate for the streamwise length scale emerges:

$$\lambda_x^+ \simeq 2140. \tag{3}$$

This result is in close agreement with the scale ($\lambda_x^+/2 \simeq 1300$) deduced from two-point space-time correlation measurements of wall shear stress fluctuations from Kreplin and Eckelmann (1979).

For a growing laminar shear layer, the critical thickness which corresponds to instability is:

$$\left(\frac{\delta u_\tau}{\nu}\right)_{\text{crit}} \simeq 35. \tag{4}$$

This value compares well with the most probable location where breakdown of the low-speed streaky structure occurs leading to the bursting event which, according to Kline et al. (1967), contributes to a large portion of the turbulence production near the wall. Using different conditional sampling schemes to detect the bursting process, Jovanović (1984) could show that the mean interval between the bursts reaches a minimum value at the edge of the buffer region $x_2^+ \simeq 30$.

To gain additional insight into the interconnection between the mechanisms leading to transition and of the continuous generation of turbulence near the wall, we may use the wave propagation velocity c_r and the wavelength λ of the disturbances at the instability point (see Schlichting, 1968):

$$c_r \simeq 0.42U_\infty, \quad \lambda \simeq 17.5\delta_1 \tag{5}$$

to estimate the time scale

$$T_B \sim \frac{\lambda}{c_r} \tag{6}$$

of the periodic events leading to the bursting process. Using (5) and (6) it can easily be shown that

$$\frac{T_B u_\tau^2}{\nu} \simeq 12 \quad \text{and} \quad \frac{\lambda u_\tau}{\nu} \simeq 210. \tag{7}$$

The above results are in close agreement with the data obtained from simultaneous flow visualization and hot-wire measurements by Falco and Gendrich (1989). These results suggest that low-speed streak lifting, oscillation and breakdown are triggered by the vortex-ring type structure of a mushroom cross-sectional shape which Falco (1977) named typical eddy. It scales on inner variables rather than on the shear layer thickness and is responsible for the transitional instability close to the wall.

3. Anisotropy invariant mapping

In the near-wall region of turbulent flows the anisotropy of turbulence plays a very important role since the turbulence energy is not distributed equally between all three fluctuating components. The analysis of the Reynolds number dependences requires the application of the invariant theory since changes in the Reynolds number may be reflected in changes in the anisotropy. The anisotropy of the turbulence can be quantified, according to Lumley and Newman (1977), using the anisotropy tensor:

$$a_{ij} = \frac{\overline{u_i u_j}}{q^2} - \frac{1}{3}\delta_{ij}$$

and its scalar invariants:

$$II_a = a_{ij}a_{ji}, \tag{8}$$

$$III_a = a_{ij}a_{ik}a_{jk}. \tag{9}$$

A plot of (8) versus (9) for axisymmetric turbulence:

$$II_a = \frac{3}{2}\left(\frac{4}{3}|III_a|\right)^{2/3}$$

and two-component turbulence:

$$II_a = \frac{2}{9} + 2III_a$$

defines the anisotropy invariant map according to Lumely (1978). In Fig. 2(a), the asymptotic states of turbulence are shown. These span an area between three points which bound all physically realizable turbulence. Invariant theory tries to describe all important features of dynamic behaviour of turbulence by the invariants II_a and III_a. Turbulence states which are close to each other in the invariant map are assumed to show similar physical behaviour. Therefore, it is possible to express modelling parameters as functions of the anisotropy invariants.

Jovanović et al. (1995, 1999) proposed the following strategy to improve the modelling of turbulent flows. Owing to additional symmetries, he argued that the modelling parameters can be specified in the asymptotic states of turbulence by analytical considerations and by evaluation of DNS data. The value Y of a parameter inside the invariant map is then computed by application of an interpolation scheme:

$$Y = (1-F)(Y)_{2C} + F(Y)_{\text{axi}}, \tag{10}$$

where F is the interpolation function

$$F = \frac{1 - 9((1/2)II_a - III_a)}{1 - 9\left[(3/4)((4/3)|III_a|)^{2/3} - III_a\right]}. \tag{11}$$

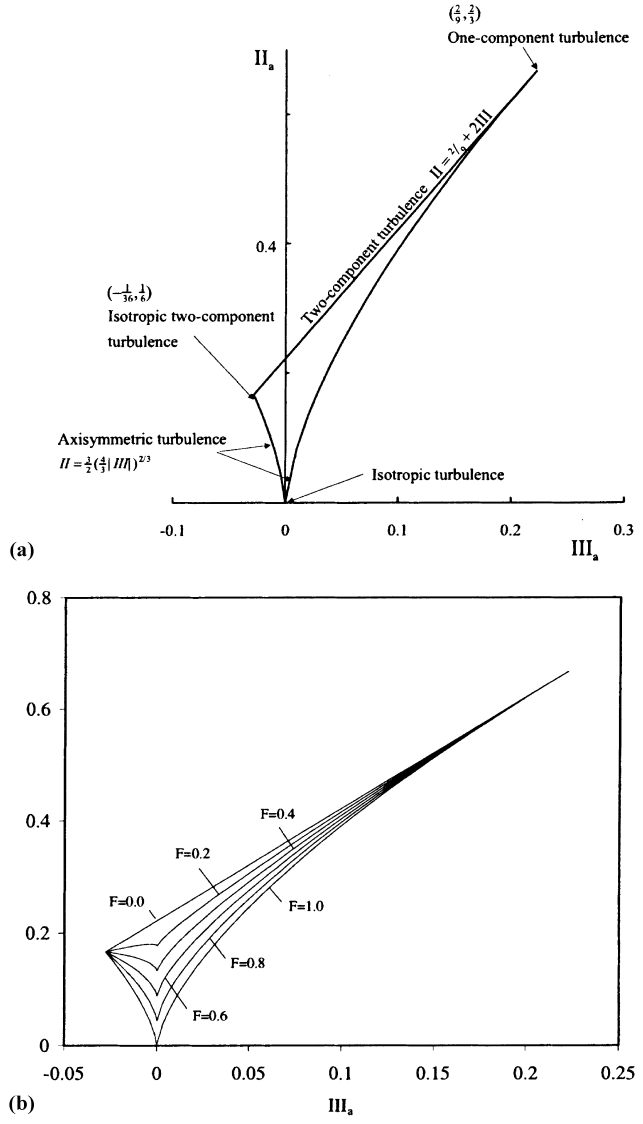

Fig. 2. Limiting states of invariant map (a) and constant values of interpolation function F (b).

Contours of constant values of the interpolation function between $F = 0$ and $F = 1.0$ inside the invariant map are shown in Fig. 2(b).

4. Analysis of DNS data

The utilization of the numerical databases may give some insight into the mechanisms of turbulent wall-bounded flows.

4.1. Energy balance

In the following we examine the influence of Reynolds number on the terms in the budget for the turbulence kinetic energy $k = 1/2\overline{u_s u_s}$:

$$\frac{\partial k}{\partial t} + \overline{U}_k \frac{\partial k}{\partial x_k} = \underbrace{-\overline{u_i u_k}\frac{\partial \overline{U}_i}{\partial x_k}}_{P_k} \underbrace{-\frac{1}{2}\frac{\partial}{\partial x_k}\overline{u_s u_s u_k}}_{T_k} \underbrace{-\frac{1}{\rho}\frac{\partial}{\partial x_i}\overline{p u_i}}_{\Pi_k} \underbrace{-\nu\overline{\frac{\partial u_i}{\partial x_k}\frac{\partial u_i}{\partial x_k}}}_{\epsilon} + \underbrace{\nu\frac{\partial^2 k}{\partial x_k \partial x_k}}_{D_k}. \quad (12)$$

Since the influence of convection is negligible, the balance of (12) consists of production (P_k), turbulent (T_k) and pressure (Π_k) transport, dissipation (ϵ) and viscous diffusion (D_k). All turbulence kinetic energy produced in the flow is converted to heat by the dissipation process. Therefore, the integral over the sum of both terms must vanish:

$$\int_0^h (P_k - \epsilon)\, \mathrm{d}x_2 = 0. \quad (13)$$

The other three terms in Eq. (12) basically describe the transport of energy normal to the mean flow direction. It turns out that the viscous diffusion (D_k) is sensitive to variations in Re but plays a passive role and serves only to satisfy the boundary conditions at the wall. The turbulent (T_k) and pressure (Π_k) transport are relatively insensitive to the Reynolds number dependence. In Fig. 3 are plotted the dissipation and production rate terms for channel and boundary layer flows. The Reynolds numbers for channel flow $Re_m = 2900$, 5600 and 13 800 (based on the bulk velocity $\overline{U}_m$ and full width $H = 2h$ of the channel) and for boundary layer flow $Re_\theta = 300$, 670 and 1410 (based on the outer flow velocity U_∞ and the momentum thickness θ). For this purpose the databases of Kim et al. (1987), Kuroda et al. (1989, 1993), Horiuhi, 1992 Gilbert and

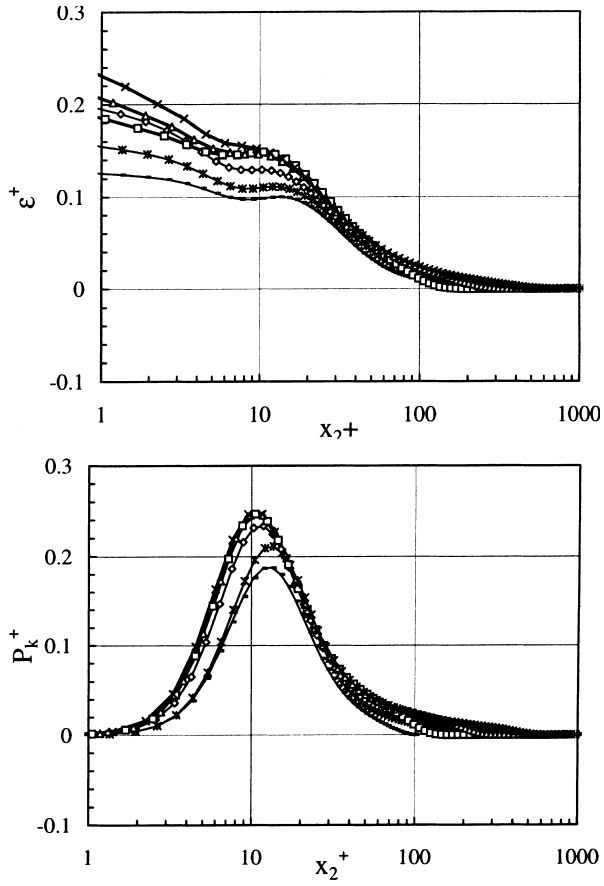

Fig. 3. Balance of the turbulence kinetic energy in plane channel flow (thin lines) and turbulent boundary layer flow (thick lines) for different Reynolds numbers. □, Kuroda et al. (1989), $Re_m = 2900$; ×, Horiuhi (1992), $Re_m = 5600$; ○, Antonia et al. (1992), $Re_m = 13800$; □, Spalart (1988), $Re_\theta = 300$; △, Spalart (1988), $Re_\theta = 670$; ×, Spalart (1988), $Re_\theta = 1410$.

Kleiser (1991), Antonia et al. (1992) and Spalart (1988) were employed.

Using the mean momentum equation, the production rate term in (12) may be expressed as follows:

$$P_k^+ = \frac{\mathrm{d}\overline{U}_1^+}{\mathrm{d}x_2^+} - \left(\frac{\mathrm{d}\overline{U}_1^+}{\mathrm{d}x_2^+}\right)^2 + f(Re_\tau), \tag{14}$$

where the last term on the right-hand side of (14), $f(Re_\tau)$, originates from the streamwise pressure gradient, which can be determined from the shear stress at the wall. Hence $f(Re_\tau) = -(x_2^+/Re_\tau)(\mathrm{d}\overline{U}_1^+/\mathrm{d}x_2^+)$ for channel flows and $f(Re_\tau) = 0$ for boundary layer flows. Re_τ is defined as $Re_\tau = u_\tau h/\nu$. As can be inferred from (14), the production term in the case of turbulent channel flows exhibits a strong Reynolds number dependence even very close to the wall. Therefore, one could argue that the source for the Reynolds number dependence of ϵ and k at the wall is the change in the production process which leads to a Reynolds number dependence of energy transported to the wall by the viscous diffusion process. This conjecture is contradicted by the result for turbulent boundary layer flows where a Reynolds number dependence of ϵ at the wall is found while the behaviour of P_k close to the wall is universal. Based on these results, one may conclude that the source of the observed low Reynolds number effects in wall-bounded flows lies in the dissipation equation.

It is interesting to analyse the influence of Reynolds number on the anisotropy of the Reynolds stresses since it can shed some light on the dynamics of turbulence in the near-wall region. In the near-wall region the invariants follow the upper boundary of the anisotropy invariant map which characterizes two-component turbulence. Fig. 4 shows the effect of Reynolds number on the anisotropy of the turbulence for channel flow. There are two noticeable trends in the data that can be clearly distinguished. First, let us look at the region very close to the wall. There, with increasing Reynolds number, the anisotropy decreases. Consequently, the invariants, which lie along the two-component limit tend to move towards the left corner point of the anisotropy map, which corresponds to the two-component isotropic state. In the buffer and logarithmic flow regions the invariants closely follow the right boundary of the anisotropy map, which corresponds to axisymmetric turbulence. From Fig. 4 it appears that with increase in Reynolds number there is a trend in the data to shift gently towards the limit valid for two-component turbulence.

We may try to use the above-mentioned inferences gained from the numerical databases in order to explain the observed low Reynolds number effects close to the wall which are concentrated in the dynamic equation for the turbulence dissipation rate. This is plausible since the dynamics of ϵ are influenced by the anisotropy of the turbulence. We shall see later how the Reynolds number dependence of ϵ at the wall actually arises.

4.2. Dissipation rate balance

In the studies of Jovanović et al. (1995, 1999), the two-point correlation technique and the invariant theory were used to examine turbulence closure for dissipation rate correlations. The results of the analysis were found to be consistent with the suggestion made by Lumely (1978) that the anisotropy of turbulence plays an important role in the budget of dissipation rate correlations. Based on these considerations, Jovanović et al. (1995, 1999) derived the following set of the equations which govern approximately the dynamics of the turbulence dissipation rate:

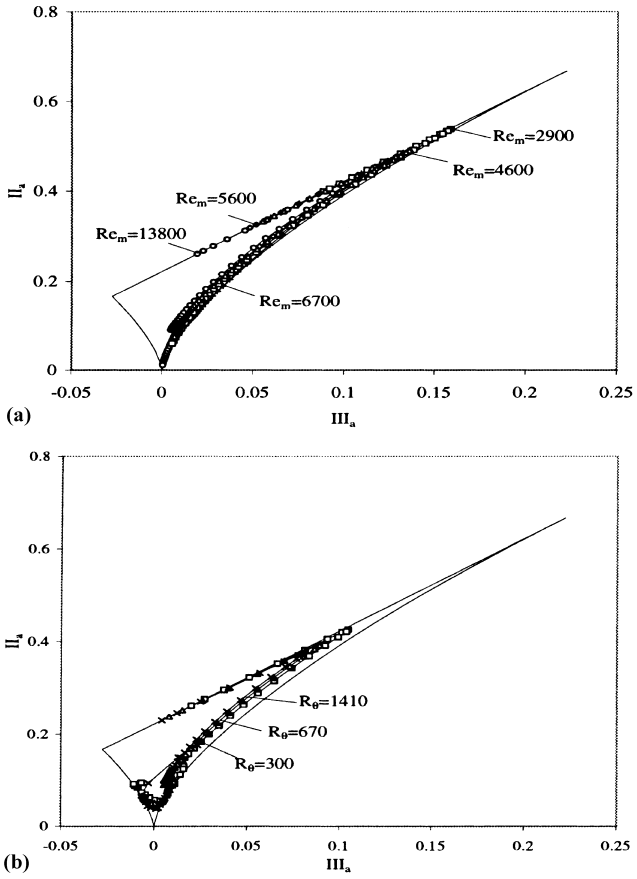

Fig. 4. Traces of the joint variations of II_a and III_a across the anisotropy invariant map. Data correspond to a plane channel flow (a) and turbulent boundary layer flows (b) at different Reynolds numbers.

$$\epsilon = \frac{1}{2}\nu\Delta_x k + \epsilon_h, \tag{15}$$

$$\frac{\partial\epsilon_h}{\partial t} + \overline{U}_k\frac{\partial\epsilon_h}{\partial x_k} = -2A\,\frac{\epsilon_h\overline{u_k u_s}}{k}\,\frac{\partial\overline{U}_s}{\partial x_k} - \psi\frac{\epsilon_h^2}{k} + \frac{\partial}{\partial x_k}\left(C_\epsilon\frac{k}{\epsilon_h}\overline{u_k u_l}\frac{\partial\epsilon_h}{\partial x_l}\right) + \frac{1}{2}\,\nu\Delta_x\epsilon_h. \tag{16}$$

According to (15), the turbulence dissipation rate ϵ is composed of an inhomogeneous part $1/2\nu\Delta_x k$ and a homogeneous part ϵ_h. The homogeneous part of the dissipation rate ϵ_h is directly related to the Taylor microscale λ as $\epsilon_\mathrm{h} = 5\nu q^2/\lambda^2$.

The first two terms on the right-hand side of (16) approximate the production of ϵ_h by the mean velocity gradient. Examination of the limiting behaviour of the two-point velocity correlation for the various states of turbulence permitted the closure for the generation of ϵ_h to be expressed in terms of the anisotropy of turbulence and turbulent Reynolds number:

$$-2A\frac{\epsilon_h}{k}\overline{u_k u_l}\frac{\partial\overline{U}_k}{\partial x_l}, \quad A = A(II_a, III_a, R_\lambda), \quad R_\lambda = \frac{\lambda q}{\nu}.$$

In two-component turbulence and for arbitrary Reynolds number, the invariant function A has the value $A = 1$. For vanishing anisotropy and very low Reynolds numbers, $A = 1$. For small anisotropy and very large Reynolds numbers $A \simeq 0$, which is in close agreement with Kolmogorov (1941) theory of locally isotropic turbulence.

The third term on the right-hand side of (16),

$$-\psi\frac{\epsilon_h^2}{k}, \quad \psi = \psi(II_a, III_a, R_\lambda),$$

is an approximation of the difference between the turbulent production and viscous destruction the two dominant terms in the balance of the dissipation rate equation.

The fourth term on the right-hand side of (16) accounts for the turbulent transport. The most widely used closure for this term:

$$\frac{\partial}{\partial x_k}\left(C_\epsilon \frac{k}{\epsilon_h}\overline{u_k u_l}\frac{\partial \epsilon_h}{\partial x_l}\right), \quad C_\epsilon \simeq 0.18 \tag{17}$$

is analogous to the form used for the interpretation of the similar term in the energy equation. Using the scaling arguments outlined by Tennekes and Lumley (1972), Jovanović (1999) derived the alternative closure:

$$-\frac{7\sqrt{3}}{180}\frac{\partial}{\partial x_k} J f_\epsilon \frac{\epsilon_h}{k}\overline{q^2 u_k}, \quad J = J(II_a, III_a), \; f_\epsilon = f_\epsilon(R_\lambda). \tag{18}$$

In contrast to (17), the use of (18) permits a nearly perfect balance of the dissipation rate equation to be obtained from the experimental data measured near the centreline of a plane turbulent wake flow at low Reynolds number.

The last term on the right-hand side of (16) is the viscous diffusion of ϵ_h.

Fig. 5 shows the asymptotic behaviour of the invariant functions A, ψ and J used to approximate the influence of the anisotropy of turbulence on the source, sink and transport processes in the dynamic equation for ϵ_h. The asymptotic values of the invariant functions A, ψ and J at three corner points of the anisotropy invariant map can be matched together using the invariant theory. Based on the these considerations, the reformulated closure of the dissipation rate equation given by (15) and (16) can cover the entire anisotropy invariant map, i.e. all physically realizable turbulence.

We may now examine the closure of the ϵ_h Eq. (16) with the aim of isolating the cause of the previously described Reynolds number variation of ϵ near the wall. In the region of viscous sublayer, the decay term $(-\psi\epsilon_h^2/k)$ of the dissipation rate equation is balanced by the viscous diffusion term $((1/2)\nu\Delta_x\epsilon_h)$. For this reason, only an increase in ψ can raise the viscous diffusion and also ϵ at the wall. However, the trend in the data extracted from numerical simulations indicates that the anisotropy of turbulence at the wall decreases with increasing Reynolds number. This trend implies a decrease in ψ and ϵ at the wall with increasing Reynolds number.

However, the above consideration does not account for the effects of the dimensionality of turbulence close to the wall. As the wall is approached the normal velocity component vanishes much faster than other two components and the flow is forced to move in the planes which are parallel to the wall. Thus, to a first approximation, turbulence in the viscous sublayer might be considered as two-component and two-dimensional. For such a state ψ may be approximated in the form $\psi_{2C-2D} \simeq 0.02R_\lambda$. This form eliminates singularity in the sink term of the dissipation equation when it is applied to the flow predictions close to the wall. Therefore, we may conclude that *the behaviour of* $(\psi)_{2D-2C}$ *very close to the wall is responsible for the rise in* ϵ *at the wall with increasing Reynolds number.*

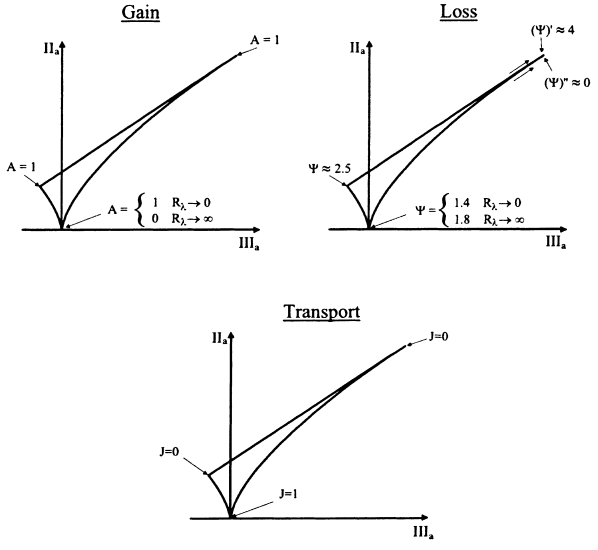

Fig. 5. Limiting values of the invariant functions A, ψ and J for the different states of turbulence (Jovanović, 1999).

5. Experimental investigations

From the analysis carried out the reader may come to the conclusion that the numerical databases form a firm basis for investigating the dynamics of turbulence in a channel flow and that there is no need for the additional experimental data in order to clarify the low Reynolds number effects close to the wall. However, examination of the budget of the dissipation rate equation close to the wall reveals noticable discrepancies between the numerical databases in the near-wall region.

For the above reason, it is desirable to perform additional measurements under well-controlled laboratory conditions and at similar Reynolds numbers as these provide flow information which is independent of numerical limitations.

To study the low Reynolds number effects in fully developed plane channel flows, a water flow facility was set up which permitted mean velocities of up to 2.5 m/s to be obtained. The channel test section of dimensions $l \times b \times H = 1\text{ m} \times 0.18\text{ m} \times 0.01\text{ m}$ was preceded by a rectangular contraction chamber ($0.15 \times 0.18\text{ m}^2$). The measurements were performed 71 channel heights downstream of the inlet using a laser-Doppler anemometer. Two different LDA systems were used in the present study in order to ensure good spatial and temporal resolution of the measurements. The data were arrival-time averaged under well-controlled seeding conditions in order to minimize the effects of velocity biasing. Those data for which the probability density for the detection at different wall distances inside the control volume were not plotted ($x_2 < 3/2d_2$).

To study the laminar-to-turbulent transition in a boundary layer a 10 mm thick flat plate was installed in the 400 kW wind tunnel at LSTM-Erlangen. The closed test section has dimensions of 1.87 m × 1.4 m. The background turbulence could be reduced to $u_1'/\overline{U}_1 \approx 0.08\%$ and $u_2'/\overline{U}_1 \approx 0.04\%$, respectively. In order to promote the boundary layer transition a rectangular, two-dimensional roughness element of 1.1 mm height was mounted at a distance of 0.31 m from the leading edge. The measurements were undertaken with a DANTEC two-component LDA probe.

5.1. LDA control volume effects

Owing to the spatial distribution of turbulent fluctuations, the Doppler shift frequency obtained from each scattering particle does not correspond to the velocity in the centre of the measuring control volume but represents the time and volume integrated information. Durst et al. (1998) derived equations

for the correction of control volume effect statistical properties. Former approaches to correct control volume effects have suggested that the detection probability is proportional to the distribution of the light intensity in the control volume. In the following the ellipsoidal shape of the control volume and the discreteness of particle detection will be taken into account.

Mean and the fluctuating parts of the velocity may be expanded in Taylor series as follows:

$$U_i = \overline{U}_i + u_i, \tag{19}$$

$$\overline{U}_i = \overline{U}_{i,c} + \sum_{n=1}^{\infty} \frac{1}{n!} \left(\frac{\partial^n \overline{U}_i}{\partial x_j^n} \right)_c (x_j - x_{j,c})^n, \tag{20}$$

$$u_i = u_{i,c} + \sum_{n=1}^{\infty} \frac{1}{n!} \left(\frac{\partial^n u_i}{\partial x_j^n} \right)_c (x_j - x_{j,c})^n. \tag{21}$$

If one decomposes the instantaneous velocity into mean and fluctuating parts along the particle trace and across the entire control volume, a relationship between measured quantities and those corresponding to the centre of the control volume arises:

$$\overline{U}_i(x_{1,c}, x_2, x_3) + u_i(x_{1,c}, x_2, x_3, t) = \overline{U}_{i,c_v} + u_{i,c_v}(t). \tag{22}$$

Volume and time integration procedure (see Durst et al., 1995) yields the following corrections for mean velocity and turbulence intensity:

$$\overline{U}^+_{i,c_v} \approx \overline{U}^+_{i,c} + \frac{d_2^{+2}}{32} \left(\frac{\partial^2 \overline{U}^+_i}{\partial x_2^{+2}} \right)_c,$$

$$\overline{u^{+2}_{i,c_v}} \approx \overline{u^{+2}_{i,c}} + \frac{d_2^{+2}}{32} \left[2 \left(\frac{\partial \overline{U}^+_i}{\partial x_2^+} \right)_c^2 + \left(\frac{\partial^2 \overline{u_i^{+2}}}{\partial x_2^{+2}} \right)_c \right], \tag{23}$$

where d_2 is the minor axis of the control volume, which is assumed to be ellipsoidal in shape.

The measured mean velocity is very close to the time-averaged value at the centre of the measuring control volume since the correction depends only on the second derivative of the mean velocity profile, which is negligible in close proximity of the wall.

The correction for the turbulence intensity is proportional to the mean velocity gradient and curvature of the intensity profile near the wall. The sum of both terms increases the measured intensity in comparison with the value at the center of the measuring control volume. Analysis of the limiting behaviour of (23) by means of Taylor series expansions:

$$\overline{u^{+2}_{1,c_v}} \approx \overline{u^{+2}_{1,c}} + \frac{d_2^{+2}}{16} \left[1 + \left(\frac{\overline{u_1^2}}{\overline{U_1^2}} \right)_{\text{wall}} \right] \tag{24}$$

together with the wall limit $\lim_{x_2 \to 0}(u_1'/\overline{U}_1) \approx 0.4$ shows that the second term in (23) contributes about 16% of the total correction.

Similarly to the above derivations, corrections can also be derived for the higher order moments. The correction for the third-order statistical moment has two relevant additional correction terms:

$$\overline{u^{+3}_{i,c_v}} \approx \overline{u^{+3}_{i,c}} + \frac{6 d_2^{+2}}{32} \left[\left(\frac{\partial \overline{U}^+_i}{\partial x_2^+} \right)_c \left(\frac{\partial \overline{u_i^{+2}}}{\partial x_2^+} \right)_c \right] + \frac{d_2^{+2}}{32} \left[+ \left(\frac{\partial^2 \overline{u_i^{+3}}}{\partial x_2^{+2}} \right)_c \right]. \tag{25}$$

The correction for the fourth-order moment contains three contributions that cannot be neglected:

$$\overline{u^{+4}_{i,c_v}} \approx \overline{u^4_{i,c}} + \frac{3 d_2^{+2}}{8} \left(\frac{\partial \overline{U}^+_i}{\partial x_2^+} \right)_c^2 \overline{u^{+2}_{i,c}} + \frac{d_2^{+2}}{32} \left[8 \left(\frac{\partial \overline{u_i^{+3}}}{\partial x_2^+} \right)_c \left(\frac{\partial \overline{U_i^+}}{\partial x_2^+} \right)_c + \left(\frac{\partial^2 \overline{u_i^{+4}}}{\partial x_2^{+2}} \right)_c \right]. \tag{26}$$

In general, the volume corrections become more complicated for the higher-order moments.

Before the measurements we shall utilize the numerical database of Gilbert and Kleiser (1991) in order to simulate the influence of the LDA control volume size on measurements of the turbulence intensity and higher-order moments and the skewness $S = \overline{u^3_{1,c_v}}/u'^3_{1,c_v}$ and flatness $F = \overline{u^4_{1,c_v}}/u'^4_{1,c_v}$ factors.

Fig. 6 indicates that the dimensions of the LDA control volume can increase significantly the measured intensity near the wall. The data presented in Fig. 6 are plotted up to the minimum distance that corresponds to half of the diameter of the LDA control volume from the wall. Analysis of the results shows that the correction is strongly influenced by the term proportional to the gradient of the mean velocity. In this context it is interesting to note that the second term in (23) decreases the amount of correction in the buffer region.

The influence of the finite size of the LDA measuring control volume on the higher-order moments is displayed in Fig. 7. Since the correction procedure outlined above was applied to both the denominator and the numerator of the skewness and flatness factors, it turned out that the overall corrections are small. Fig. 7(a) suggests that with increase in the LDA control volume one can expect only a modest increase in the measured skewness factor across the viscous sublayer. The data in Fig. 7(b) imply that corrections for measurements of the flatness factor are negligible if the distance from the wall is smaller than the diameter of the measuring control volume.

The above analysis reveals that the intensity measurements are primarily influenced by spatial integration of the LDA signals across the measuring control volume.

As described in the previous sections, the diameter of the measuring control volume d_2 enters into the derived corrections. The procedures suggested in the literature (see, for example, Durst et al., 1995) for correcting laser-Doppler measurements taken in flow regions with high velocity gradients usually deduce the effective diameter of the control volume from the Gaussian light intensity distribution. However, this approach ignores the evidence that detection of the burst is

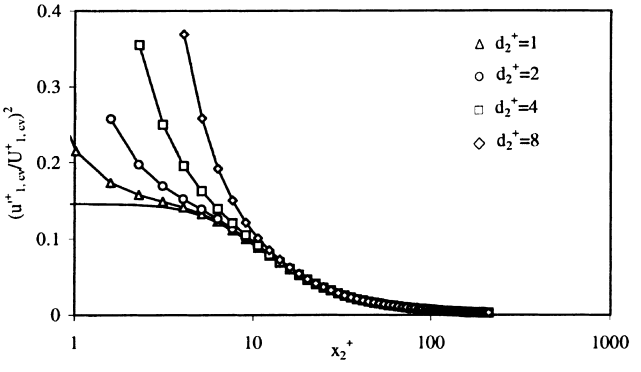

Fig. 6. Influence of the finite size of the LDA control volume on turbulence intensity measurements.

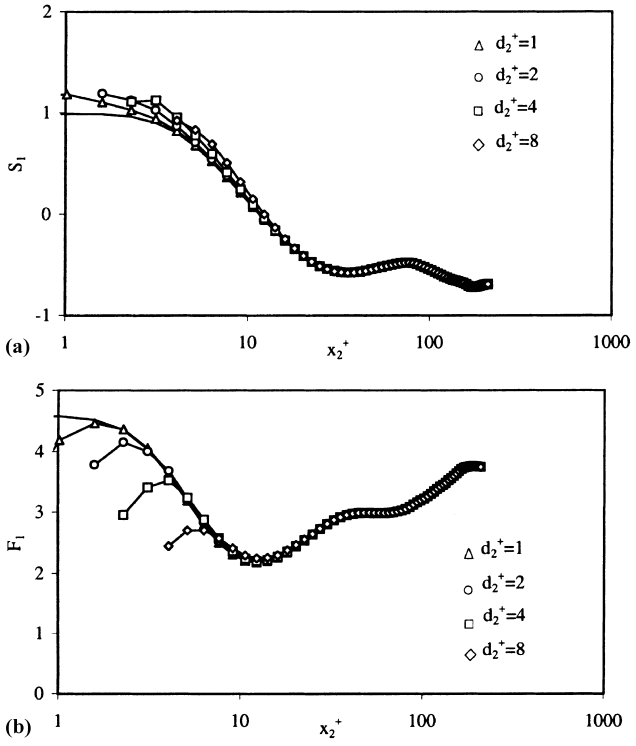

Fig. 7. Influence of the LDA control volume size on the measurements of the higher-order moments: skewness factor (a); flatness factor (b).

dependent on the scattered particle size, transmitting and receiving optical system, gain and trigger level setting in the signal processing electronics used to measure the Doppler frequency.

To obtain a confident estimate of the measuring control volume diameter, it is desirable to perform measurements in a laminar flow. Since in such a flow there are no turbulence fluctuations, the measured intensity is defined by the mean velocity gradient and the volume diameter:

$$u'^2_{1,c_v} \approx u'^2_{\text{noise, optics}} + \frac{d_2^2}{16}\left(\frac{\partial \overline{U}_1}{\partial x_2}\right)^2_c. \tag{27}$$

Here $u'^2_{\text{noise,optics}}$ stands for the noise contribution which originates from limited resolution of the burst frequency measurements and due to non-parallelism of the fringes in the LDA control volume. Fig. 8 shows that the noise contribution can be easily measured at the channel centreline.

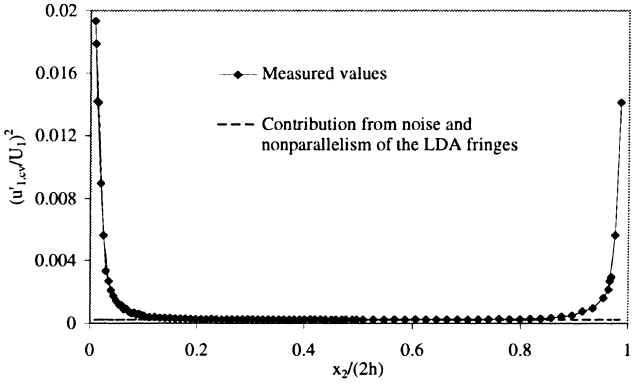

Fig. 8. Distribution of the measured intensity in a laminar channel flow.

Hence, all quantities except the effective control volume size can be measured and it is possible to determine d_2 in a laminar channel flow from the comparison of the mean flow gradient and the measured fluctuation level.

5.2. Channel flows

The measurement of streamwise turbulence fluctuations gives an insight into the influence of Reynolds number on $(\epsilon^+)_{\text{wall}}$. In Fig. 9 the RMS values of the corrected data are shown. For the evaluation of the wall limiting values of the turbulence level, the near-wall data in the region $y^+ < 10$ were extrapolated to the wall position. In Fig. 10 the resulting values extracted from the measurements are plotted against Reynolds number (among others from Mansour et al., 1998). Comparison between experiment and DNS results reveals the same trend but a considerable deviation in the absolute values of u'/U at higher Reynolds numbers. A supplementary note may be added on the low Reynolds number effects close to the wall by applying the perturbation technique (see Yajnik, 1970; Afzal and Yajnik, 1973; Philips, 1987). Using the inner length scale v/u_τ and the half-width h of the channel, a small parameter ε can be formulated as follows:

$$\varepsilon = \frac{v/u_\tau}{h} = \frac{1}{Re_\tau}. \tag{28}$$

The appropriate asymptotic expansion for $\lim_{x_2 \to 0} u'_1/\overline{U}_1$ in terms of ε reads

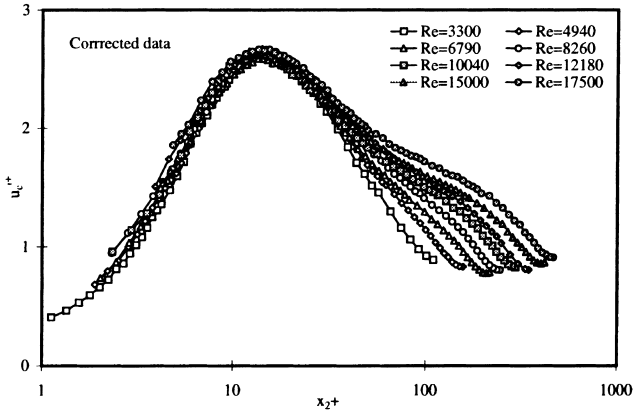

Fig. 9. Profiles of the RMS values of turbulence fluctuations.

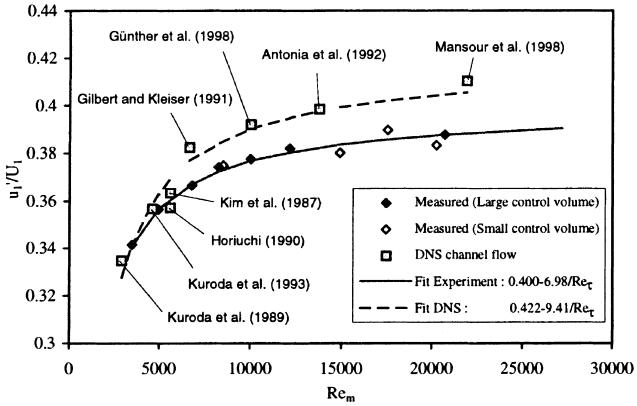

Fig. 10. Plot of determined wall limiting values for u'/U. Comparison with DNS data.

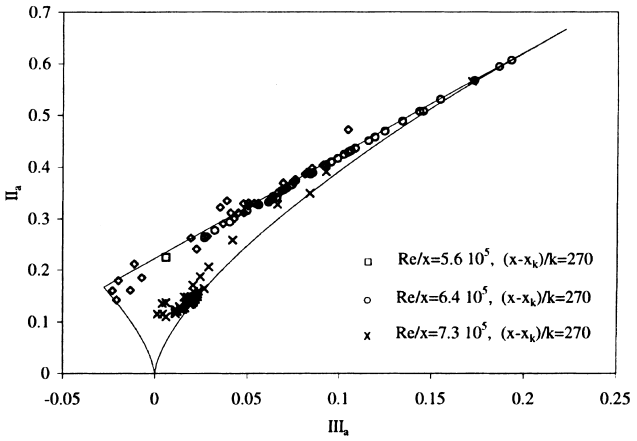

Fig. 11. Traces of the joint variations of II_a and III_a across the anisotropy invariant map. Data correspond to transitional boundary layer flow at different velocities U_∞.

$$\left(\frac{u_1'}{\overline{U}_1}\right)_{x_2\to 0} \simeq a + \frac{b}{Re_\tau} + \frac{c}{Re_\tau^2} + \cdots \tag{29}$$

and is in close agreement with the proposal suggested by Gersten (1997). The leading order term a represents the inviscid limit ($Re \to \infty$) and the higher-order terms $b, c, \ldots$ take into account low Reynolds number effects.

5.3. Boundary layer flows

The results of near-wall turbulent flows seem to imply a dynamic connection between the variations of the invariants in wall-bounded turbulent flows and the process of laminar–turbulent transition.

With this aim in mind we extend the analysis of laminar–turbulent transition process using the tools of invariant theory and the anisotropy invariant mapping. The goal is to gain some insight into the dynamics of two-component turbulence. Fig. 11 shows the values of the anisotropy invariants II_a and III_a for boundary layer profiles at the same position $x - x_k = 0.3$ m for different outer flow velocities between $U_\infty = 8.5$ and 11.0 m/s. For smaller Reynolds numbers the data are located in the vicinity of the two-component limit. This can be understood as a confirmation of the presence of Tollmien–Schlichting waves since the spanwise turns out to be very small in the two-component limit. With increasing Reynolds number and the appearance of intermittency effects, the data tend towards the one-component state of turbulence. Further increase in the Reynolds number leads to the development of turbulent boundary layer profiles, which is reflected in a movement away from the two-component limit. The data close to the wall remain in the two component state of turbulence. The results show that boundary layer transition can be treated in the frame of the invariant theory. They can serve as a basis for the preparation of a model which describes the transitional flow state.

6. Conclusions

The previous sections have presented analytical results supported by numerical and experimental data in the Reynolds number range between 3000 and 25 000. Both of these data sets reveal similar trends with increasing Reynolds number. The wall limit of $u_1'/\overline{U}_1$ high Reynolds numbers turns out to be 0.4. This value can be used as a criterion that turbulence models at the wall have to satisfy. Statistical analysis shows that the decay term of the dissipation rate equation is responsible for the low Reynolds number effects at the wall.

Away from the very near-wall region, the Reynolds number dependence of the turbulence statistics is caused by the streamwise pressure gradient which contributes to the production processes in the equations for the turbulence kinetic energy and turbulence dissipation rate. Anisotropy invariant mapping of the Reynolds stress tensor reveals a tendency for the turbulence statistics to shift slightly from nearly axisymmetric state towards the two-component state. This trend implies a gentle increase of the turbulence dissipation rate in the buffer and logarithmic flow regions with increasing Reynolds number. Combined application of analytical and experimental approaches has resulted in an improved insight into the mechanisms of Reynolds number effects on turbulence fluctuations near solid walls.

Acknowledgements

This research received financial support through the Deutsche Forschungsgemeinschaft within the project Du 101/49-1 and Du 101/54-1. The authors gratefully acknowledge this support of their work.

References

Afzal, N., Yajnik, K., 1973. Analysis of turbulent pipe and channel flows. J. Fluid Mech. 61, 23–31.

Antonia, R.A., Teitel, M., Kim, J., Browne, L.W.B., 1992. Low-Reynolds number effects in a fully developed channel flow. J. Fluid Mech. 236, 579–605.

Durst, F., Jovanović, J., Sender, J., 1995. LDA measurements in the near-wall region of a turbulent pipe flow. J. Fluid Mech. 295, 305–355.

Durst, F., Fischer, M., Jovanović, J., Kikura, H., 1998. Methods to set up and investigate low Reynols number, fully developed turbulent plane channel flows. J. Fluid Eng. 120, 496–503.

Fage, A., Townend, H.C.H., 1932. An examination of turbulent flow with an ultramicroscope. Proc. R. Soc. A 135, 656–677.

Falco, R.E., 1977. Coherent motions in the outer region of turbulent boundery layers. Phys. Fluids 10, 124–133.

Falco, R.E., Gendrich, C.P., 1989. The turbulence burst detection algorithm. In: Kline, S.J., Afgan, N.H. (Eds.), Near-Wall Turbulence, 1988. Z. Zarić Memorial Conference. Hemisphere, New York.

Gersten, K., 1997. Personal Communication.

Gilbert, N., Kleiser, L., 1991. Turbulence model testing with the aid of direct numerical simulation results. In: Proceedings of the Eighth Symposium on Turbulent Shear Flows, 9–11 September, TU Munich, pp. 26.1.1–26.1.6.

Hinze, O.J., 1975. Turbulence, second ed. McGraw-Hill, New York, p. 600.

Horiuhi, K., 1992. Establishment of the DNS database of turbulent transport phenomena. Rep. Grants-in-aid for Scientific Research No. 02302043.

Jovanović, J., 1984. Stastical analysis and structure of wall turbulence, Dissertation, Faculty of Mechanical Engineering, University of Belgrade.

Jovanović, J., 1999. Studying turbulence using invariant theory and the numerical databases. Kurzlehrgang Turbulenz, 26–29 April 1999, LSTM Erlangen.

Jovanović, J., Ye, Q.-Y., Durst, F., 1995. Statistical interpretation of the turbulent dissipation rate in wall-bounded flows. J. Fluid Mech. 293, 321–347.

Kim, H.T., Kline, S.J., Reynolds, W.C., 1971. The production of turbulence near smooth wall in a turbulent boundary layer. J. Fluid Mech. 50, 133–160.

Kim, J., Moin, P., Moser, R., 1987. Turbulence statistics in fully developed channel flow at low Reynolds number. J. Fluid Mech. 177, 133–166.

Kline, S.J., Reynolds, W.C., Schraub, F.A., Runstadlet, W.P., 1967. The structure of turbulent boundary layers. J. Fluid Mech. 30, 741–773.

Kolmogorov, A.N., 1941. Local structure of turbulence in an incompressible fluid at very high Reynolds numbers. Dokl. Akad. Nauk SSSR 30, 299–303.

Kreplin, H., Eckelmann, H., 1979. Behavior of three fluctuating velocity components in wall region. Phys. Fluids 22, 1233–1239.

Kuroda, A., Kasagi, N., Hirata, M., 1989. A direct numerical simulation of fully developed turbulent channel flow. In: Proceedings of the International Symposium on Computational Fluid Dynamics, Nagoya, pp. 1174–1179.

Kuroda, A., Kasagi, N., Hirata, M., 1993. Direct numerical simulation of the turbulent plane Couette-Poiseulle flows: Effect of mean shear on the near wall turbulence structures. In: Proceedings of the Ninth Symposium on Turbulent Shear Flows, Kyoto, Japan, 16–18 August, pp. 8.4.1–8.4.6.

Lumely, J.L., 1978. Computational modeling of turbulent flows. Adv. Appl. Mech. 18, 123–176.

Lumley, J.L., Newman, G., 1977. The return to isotropy of homogeneous turbulence. J. Fluid Mech. 82, 161–178.

Philips, W.R.C., 1987. The wall region of a turbulent boundary layer. Phys. Fluids 30, 2354–2361.

Schlichting, H., 1968. Boundary-Layer Theory. 6th ed. McGraw-Hill, p. 453.

Mansour, N.N., Moser, R.D., Kim, J., 1998. Fully developed turbulent channel flow simulation. AGARD Rep. no. 345.

Spalart, P.R., 1988. Direct simulation of a turbulent boundary layer up to $R_\theta = 1410$. J. Fluid Mech. 187, 61–98.

Tennekes, H., Lumley, J.L., 1972. A First Course in Turbulence. MIT Press, Cambridge, MA.

Yajnik, K.S., 1970. Asymptotic theory of turbulent shear flow. J. Fluid Mech. 42, 441–427.